Dynamic Aspects of Semiconductor Photoelectrochemistry

L. M. PETER

Department of Chemistry, The University, Southampton SO9 5NH, U.K.

Received October 30, 1989 (Revised Manuscript Received February 21, 1990)

Contents

I.	Introduction	753
II.	Steady-State Photocurrents	754
	A. Photogeneration and Collection of Minority Carriers	754
	B. Surface and Bulk Recombination	754
	C. Photocurrent Multiplication	755
III.	Non-Steady-State Photoresponse	756
	A. Collection and Trapping of Photogenerated Carriers	756
	B. Majority Carrier Capture by Surface States	757
	C. Generalized Treatment of the Non Steady State	759
IV.	Laser-Induced Photocurrent Transients	759
V.	Photocurrent Response to Chopped Illumination	762
VI.	Intensity-Modulated Photocurrent Spectroscopy	764
VII.	Non-Steady-State Analysis of Photocurrent Multiplication	766
VIII.	Conclusions and Outlook	768

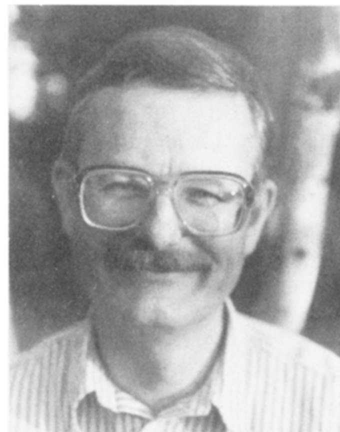

L. M. Peter was born in 1944 in Alton, England. After gaining his first degree in chemistry at the University of Southampton in 1966, he was nearly persuaded to become an organic chemist but was saved in the nick of time from such an unhappy fate by Professor (now Sir) Graham Hills, who introduced him to the mysteries of electrochemistry. This involved him in spending 3 years with his arms inserted into large neoprene drybox gloves in order to find out more about electrode processes in aprotic solvents. Undiscouraged by such sensory isolation, he received his Ph.D. in 1969 and moved first to the Technical University of Munich and then to the Fritz Haber Institute in Berlin to work as a CIBA Research Fellow with Professor Heinz Gerischer, dividing his attention between learning to ski and studying energy and charge transfer in molecular crystals. It was here that he realized that smart electrochemists shine light on their electrodes. Returning to Southampton in 1975, he began to work on the electrochemistry of semiconductors and was appointed first as Lecturer and then to his current post as Senior Lecturer. His spare time is spent on sailing a dinghy (badly), skiing (more proficiently), and cooking (enthusiastically but irreproducibly).

I. Introduction

Progress in understanding the kinetics and mechanisms of electrode processes has depended to a large extent on the development of *nonstationary techniques* that involve measurement of the potential or current response to transient or periodic excitation. In the case of metal electrodes, the main objective of nonstationary methods is to deconvolute the kinetics of electron transfer from other processes such as mass transfer or coupled chemical reactions. The upper limit of time resolution is generally set by the RC time constant of the series combination of the electrolyte resistance and the capacitance of the electrical double layer, and it is difficult to obtain reliable data for times shorter than 1 μs.[1,2] In view of the widespread acceptance of transient and periodic techniques in electrochemistry, it is surprising that they have not been used more extensively to characterize semiconductor electrodes. Much of the experimental work in semiconductor electrochemistry has been based on steady-state methods such as the measurement of photocurrent–voltage curves, and nonstationary methods have probably received less attention than they deserve. Recently, however, nonsteady-state techniques[3] have begun to make an increasingly important contribution to advances in semiconductor photoelectrochemistry, and it is therefore appropriate to review them here.

It is worth highlighting a fundamental difference between metal and semiconductor electrodes at this point. The rate constants of electrode processes at the metal/solution interface can be controlled easily because the activation energy depends directly on the potential difference across the Helmholtz layer.[4] The kinetics of electron-transfer processes can therefore be studied by perturbing the potential and measuring the transient or periodic current response of the system. However, the situation is less favorable in the case of a semiconductor electrode under depletion conditions, because most of the potential drop is located in the solid.[5] As a consequence, the main effect of changing the potential in the absence of illumination is to alter the equilibrium density of electrons and holes at the surface, whereas the rate constants for electron exchange with the redox system remain essentially unchanged.[5-8] This means that the experimental methods based on potential perturbations that have been developed to study electron transfer at metal electrodes are usually of little use for semiconductors. Although it is not easy to perturb the rate constants for electron transfer at the semiconductor/electrolyte interface, it is possible to control the rate at which nonequilibrium charge carriers are generated and collected. In pho-

0009-2665/90/0790-0753$09.50/0 © 1990 American Chemical Society

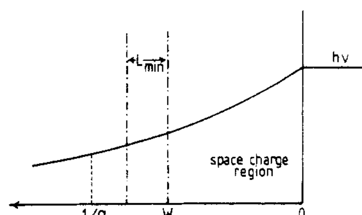

Figure 1. Intensity profile for light absorption at the semiconductor/electrolyte interface. The characteristic lengths appearing in the Gartner equation are identified in the figure. Key: W = width of the space charge region; $1/\alpha$ = penetration depth of the light (α is the absorption coefficient); L_{min} = diffusion length of minority carriers in the bulk.

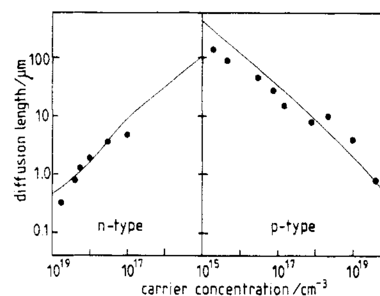

Figure 2. Diffusion length of minority carriers in n- and p-type GaAs as a function of doping density. Conditions: points experimental; lines calculated from lifetime data (data taken from ref 12).

toelectrochemistry, we are dealing with *minority carriers* (i.e., holes in n-type materials and electrons in p-type materials), and these must be generated by illumination and then collected from the bulk of the semiconductor by diffusion and migration before charge transfer can occur at the interface.[9] It follows that systems can be perturbed by short light flashes or by other time-dependent variations in light intensity. The electrical response can be followed either at open circuit, in which case a *photopotential* is recorded, or under controlled-potential conditions, when a *photocurrent* transient is observed. Alternative methods for following the fate of photogenerated carriers include measuring the transient photoluminescence or microwave absorption associated with the decay of photogenerated carriers.

II. Steady-State Photocurrents

A. Photogeneration and Collection of Minority Carriers

The general principles of semiconductor photoelectrochemistry are well established in the literature,[5-10] and since they are reviewed, only a brief summary of some essential aspects will be given here.

Figure 1 illustrates the characteristic regions for the case of an illuminated n-type semiconductor under depletion conditions. The absorption of a photon in the solid produces a nonequilibrium hole in the valence band and a corresponding electron in the conduction band. The carrier pair can be separated by diffusion or by the electric field (migration), or it can recombine. In a field-free doped semiconductor, the recombination process is pseudo first order because there is a large excess of one type of carriers (i.e., it is assumed that the illumination does not change the majority carrier density significantly). The recombination process can therefore be characterized by a first-order minority carrier lifetime τ_{min}, which is sensitive to crystal purity and doping density. Minority carriers are also characterized by their diffusion coefficient D, and when considering the problem of carrier collection, it is convenient to define the majority carrier diffusion length

$$L_{min} = (\pi D \tau_{min})^{1/2} \qquad (1)$$

as a measure of the distance that a photogenerated minority carrier travels in the field-free (quasi-neutral) region before recombining. The value of L_{min} depends on doping density as shown, for example, in Figure 2 for GaAs.[11]

It can be seen from Figure 1 that the flux of minority carriers into the surface is made up from two contributions. The first arises from the diffusion of minority carriers from the field-free region into the space charge region, and it depends on the diffusion length L_{min} and on the penetration depth of the incident light. The second contribution arises from holes excited within the space charge region that migrate rapidly to the surface under the influence of the field unless they are trapped or recombine at defect states.

Once minority carriers have reached the surface, they are free to participate in electron-transfer reactions, either with redox species in solution or with the semiconductor lattice. Provided that there are no loss mechanisms and the interface acts as an ideal sink for minority carriers, the photocurrent will depend only on generation and collection. The boundary value problem corresponding to this situation was solved by Gärtner,[12] who considered the analogous solid-state semiconductor Schottky junction. In the steady state, the potential and intensity dependence of the photocurrent j_{photo} is given by

$$j_{photo}/I_0 = 1 - \exp(-\alpha W)/(1 + \alpha L_{min}) \qquad (2)$$

Here I_0 is the incident photon flux corrected for reflection, α is the absorption coefficient, and L_{min} is the diffusion length of minority carriers. The ratio j_{photo}/I_0 is the photocurrent conversion efficiency Φ. W, the width of the space charge region, is given by

$$W = (2\Delta\phi\epsilon\epsilon_0/qN)^{1/2} \qquad (3)$$

where ϵ is the relative permittivity of the semiconductor, N is the donor or acceptor density, and $\Delta\phi$ is the potential difference across the space charge region. In the absence of complications due to charging of surface states (see section III), $\Delta\phi$ can be replaced by $E - E_{fb}$, where E_{fb} is the flatband potential. Equation 2 forms the basis of a useful method for determining minority carrier lifetimes;[13,14] plots of $-\ln(1 - j_{photo}/I_0)$ against $(E - E_{fb})^{1/2}$ are expected to be linear, and α and L_{min} can be determined from the slope and intercept values. Figure 3 illustrates how this method has been used to find the diffusion length of electrons in p-GaP in contact with aqueous H_2SO_4.[13] It can be seen from the plots that significant deviations from the Gärtner equation occur at low-band bending, and the origin of this deviation is discussed in the next section.

B. Surface and Bulk Recombination

The Gärtner equation has been widely used in semiconductor photoelectrochemistry, and in most cases it

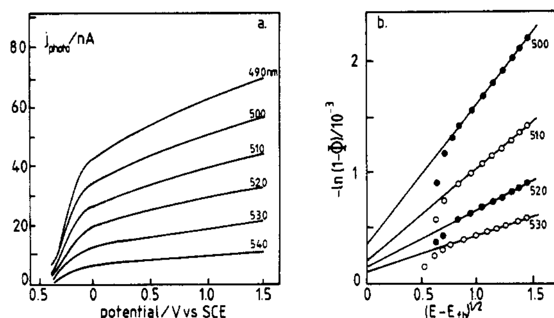

Figure 3. Determination of electron diffusion length in p-GaP: (a) set of photocurrent–voltage curves for p-GaP in 0.5 M H_2SO_4 recorded at different wavelengths; (b) data replotted according to the Gärtner equation in order to obtain the diffusion length (L_e = 7 × 10^{-6} cm) and the absorption coefficient α (λ).

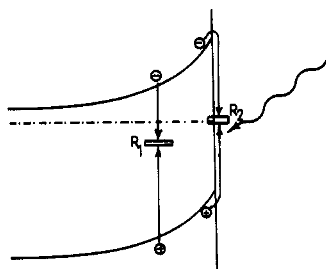

Figure 4. Photocurrent loss mechanisms. Photogenerated minority carriers can recombine either via energy levels in the bulk and space charge regions (R_1) or via surface states (R_2). In both cases, minority carrier capture results in a flux of majority carriers into the recombination zone.

gives an adequate fit to experimental photocurrent–voltage curves when $\Delta\phi$ is greater than about 0.5 V. Since loss mechanisms are neglected in its derivation, the equation represents an upper limit for the photocurrent response under normal conditions, and it is therefore not surprising that experimental photocurrent–voltage plots always deviate to some extent from the form predicted by eq 2. The photocurrent conversion efficiency is determined not only by generation and collection terms but also by electron hole recombination via energy levels in the space charge region and at the surface (surface states) as illustrated in Figure 4. Since the recombination rate depends on the density of majority carriers, the largest effects are evident at low band bending, i.e., at potentials close to flatband, where frequently no steady-state photocurrent can be detected in spite of the fact that the Gärtner equation predicts that carriers will still be collected by diffusion. The importance of recombination close to flatband is evident even in the plots in Figure 3, which were obtained at very low light intensities in order to minimize recombination effects due to photogenerated hydrogen.[13] At higher light intensities, the deviations are often much greater. Some experimental results for the n-GaAs/electrolyte interface that illustrate the effect of increasing the light intensity are shown in Figure 5.[15] Several theoretical treatments of volume and surface recombination under steady-state conditions have been presented in the literature,[8,16–21] but they fail to account correctly for the dependence on light intensity that is illustrated by Figure 5 and also observed in several other systems. The results in Figure 5 suggest that the nonideality in the photocurrent–voltage curves is connected with interfacial photoelectrochemistry leading, for example, to changes in band bending due to surface

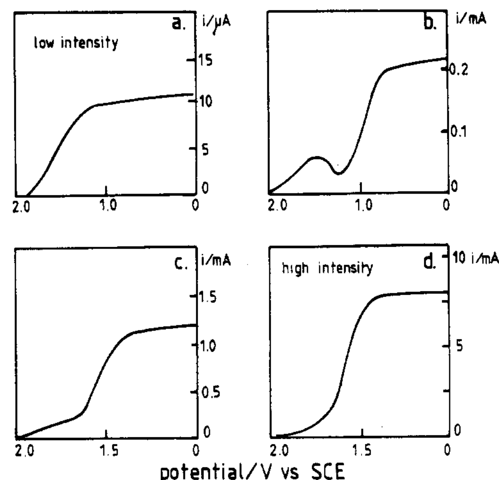

Figure 5. Photocurrent-voltage curves for n-GaAs in 0.1 M KOH/14 mM K_2Se showing the effect of increasing the light intensity from a to d. Incident photon flux values ($cm^{-2}\,s^{-1}$): (a) 2×10^{14}, (b) 4×10^{15}, (c) 3×10^{16}, (d) 4×10^{17}. Wavelength 632.8 nm. Note the way in which the photocurrent onset is displaced to more positive potentials at higher intensities as the result of recombination and changes in surface composition. The nonideality of the junction is also demonstrated by the appearance of a hump in the photocurrent-voltage curve at intermediate illumination levels.

charging or losses resulting from the formation of surface recombination centres during photocorrosion.

C. Photocurrent Multiplication

In some circumstances, measured photocurrents may exceed the upper limit set by the Gärtner equation; i.e., the quantum yield for the photocurrent is greater than unity. There are several experimental examples where the photocurrent is almost double that expected from the Gärtner equation; these include the oxidation of alcohols, aldehydes, and carboxylic acids on ZnO,[22,23] TiO_2,[24] CdS,[25] and CdSe[26] as well as the reduction of H_2O_2 on GaP[27] and of oxygen on p-GaP[28] and on p-GaAs.[29] The phenomenon is referred to as current doubling, and it involves the capture of a photogenerated minority carrier to form a reactive intermediate that can inject a majority carrier into the semiconductor. Examples for the reactions at n- and p-type electrodes are illustrated in eqs 4 and 5.

n-TiO_2

$$h\nu \rightarrow h + e^- \quad (4a)$$

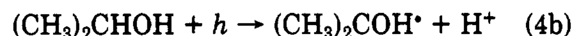

$$(CH_3)_2CHOH + h \rightarrow (CH_3)_2COH^{\bullet} + H^+ \quad (4b)$$

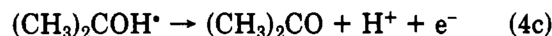

$$(CH_3)_2COH^{\bullet} \rightarrow (CH_3)_2CO + H^+ + e^- \quad (4c)$$

p-GaP

$$h\nu \rightarrow h + e^- \quad (5a)$$

$$O_2 + H^+ + e^- \rightarrow HO_2^{\bullet} \quad (5b)$$

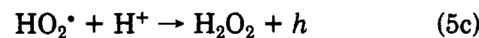

$$HO_2^{\bullet} + H^+ \rightarrow H_2O_2 + h \quad (5c)$$

Figure 6 compares the photocurrent response predicted by the Gärtner equation with the experimental result observed for GaP in oxygen-saturated solution, where current doubling occurs via reaction 5c, and in oxygen-free solution where no doubling occurs.[28] Photocurrent multiplication is also observed during the

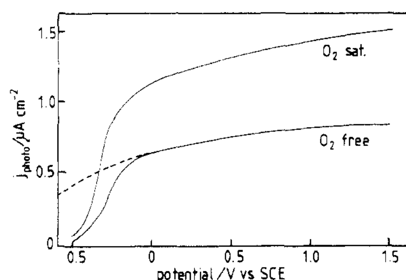

Figure 6. Photocurrent–voltage curves for p-GaP in 0.5 M H_2SO_4 showing the "current doubling" effect observed in the presence of oxygen. The broken line represents the photocurrent calculated from the Gärtner equation. The current doubling effect arises from hole injection by the $HO_2^{\bullet}$ intermediate.

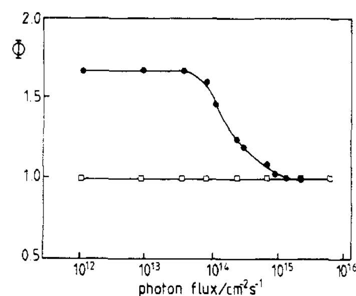

Figure 7. Intensity dependence of the photocurrent multiplication effect observed in the p-GaP/O_2 system: closed circles, O_2-saturated solution; open squares, oxygen-free solution. The multiplication effect disappears at high intensities because the $HO_2^{\bullet}$ intermediate is reduced by photogenerated electrons before hole injection can occur.

anodic dissolution of the elemental semiconductors Si[30-32] and Ge.[30] In the case of the photodissolution of n-Si in fluoride solutions, the quantum yield is reported to approach 4 under low-intensity conditions, whereas the quantum yield for Ge dissolution under the same conditions is close to 2.[30] These photocurrent multiplication processes must involve electron injection by intermediates in the lattice dissolution process. In order to explain a quantum yield of 4 in the case of silicon in fluoride solutions, it is necessary to assume that the capture of a photogenerated hole is followed by the injection of three electrons into the conduction band.[32] The non-steady-state behavior of these systems will also be considered in this review,[32-34] although work is still in progress to deconvolute the individual steps involved in lattice dissolution.

An interesting feature of the injection steps in current doubling reactions is that they must compete effectively with capture of minority carriers by the intermediate.[28,32-34] Unless the injection step is fast, the intermediate will capture a second minority carrier, as shown in eq 6 for the photoreduction of oxygen, and the overall quantum efficiency will be reduced to unity.

$$HO_2^{\bullet} + H^+ \rightarrow H_2O_2 + h \qquad (6a)$$

must compete with

$$HO_2^{\bullet} + H^+ + e^- \rightarrow H_2O_2 \qquad (6b)$$

Experimentally, competition between the two routes manifests itself as an intensity-dependent quantum efficiency; at low intensities where the density of minority carriers is low, the current multiplication route dominates. As the intensity is increased, the minority carrier density becomes so large that the intermediate no longer has time to inject a carrier before it captures a second photogenerated carrier. Figure 7 illustrates this effect for the case of oxygen reduction on p-GaP, where a full kinetic analysis of the parallel reaction scheme has been made.[28]

This brief overview of semiconductor photoelectrochemistry is intended to establish some of the areas of particular interest where dynamic measurements have provided new information. It is clear that the existence of loss or gain mechanisms can be established by quantitative measurements in the steady state, and under favorable circumstances it has even proved possible to derive kinetic information, for example on the rate of majority carrier injection by the $HO_2^{\bullet}$ intermediate in eq 5b.[28] However, further progress in understanding these processes has come about largely through the application of the perturbation methods that are described below.

III. Non-Steady-State Photoresponse

A. Collection and Trapping of Photogenerated Carriers

The transient or periodic response of the illuminated semiconductor/electrode junction arises from a number of processes taking place on different time scales. Before they are examined individually, it is necessary to distinguish two limiting experimental situations. If the illumination is very intense, for example a high-power laser pulse, more carriers may be generated by the light than were present originally. Under these conditions, the redistribution of charge modifies the potential drop across the semiconductor—in extreme cases the band bending will be reduced to zero. At lower intensity levels, on the other hand, the perturbation of the charge distribution is much smaller and Figure 1 can still be used as the basis for discussion. The collection of photoexcited minority carriers from the space charge and field-free regions of the semiconductor occurs very rapidly. The transit time for minority carriers in the space charge region is determined by the carrier mobility and the electrical field, and in the absence of trapping at bulk defect states, carriers are swept to the surface in a nanosecond or less.

When a minority carrier reaches the interface, it may be transferred directly from the band to a redox species or alternatively it may be trapped by a localized energy level located in the band gap. The rate of these processes can be expressed in terms of the thermal velocity of carriers v the capture cross section σ_t, and the surface number density N_t of the trapping or redox states:

$$s_t = v\sigma_t N_t \qquad (7)$$

s_t is often referred to as the surface recombination velocity,[35] although the term minority carrier capture velocity is probably more appropriate[36] since recombination via surface levels is a two-step process involving also capture of majority carriers. In order to gain an idea of the order of magnitude of s_t, let us assume a capture cross section of 10^{-17} cm^2, a thermal velocity of 10^7 cm s^{-1}, and a number density of 10^{12} cm^{-2}, equivalent to a concentration of redox species of about 0.1 M or a surface coverage of about 10^{-3}. The surface capture velocity is then 10^3 cm s^{-1}. This means that the surface carrier lifetime in the band is less than 100 ps.

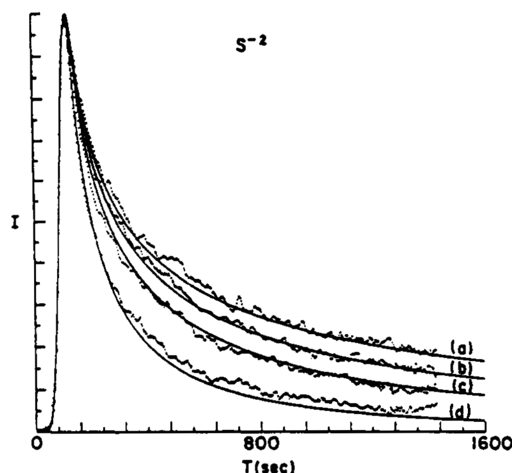

Figure 8. Experimental and simulated picosecond photoluminescence decay curves for a CdS single crystal immersed in Na_2S solution. Sulfide concentrations: (a) 0, (b) 0.3 mM, (c) 7 mM, (d) 10 mM (reproduced from ref 42; copyright 1988 American Chemical Society).

Surface recombination velocities can be measured at open circuit by following the decay of carrier density following pulsed laser excitation. Time-resolved photoluminescence measurements[37-42] have focused on the behavior of CdS crystals immersed in aqueous electrolyte solutions. The semiconductor/electrolyte interface acts as an additional sink for photogenerated carriers, adding to the bulk recombination term. The time-dependent carrier concentration $\Delta n(x,t) = \Delta p(x,t)$ is determined by the continuity equation[43]

$$\frac{\partial \Delta n(x,t)}{\partial t} = \frac{D^* \delta^2 \Delta n(x,t)}{\partial x^2} - \frac{\Delta n(x,t)}{\tau_b} + G(x,t) \quad (8)$$

where D^* is the ambipolar diffusion coefficient, τ_b is the carrier lifetime, and G is the rate of photogeneration of minority carriers. It should be noted that the transport term only takes into account diffusion; it is assumed that the light pulse is so intense that the band bending is eliminated. In practice, it is always necessary to establish that this is the case. The second term takes account of bulk recombination, which is assumed to be first order. The final term describes the position-dependent generation of carriers that follows the light absorption profile.

Benjamin and Huppert[42] were able to show that the photoluminescence decay rate for CdS is enhanced by the adsorption of sulfide ions at the CdS/electrolyte interface; their transients are shown in Figure 8. The experimental data were fitted with use of the solution of eq 8 with appropriate boundary conditions in order to determine the surface recombination velocity. In this way, Benjamin and Huppert have deduced values of s_t as high as 10^6 cm s^{-1} in the limit of high surface coverage, corresponding to a capture cross section σ_t of at least 10^{-16} cm^2. At first sight, such a high surface recombination velocity might appear to imply a low quantum efficiency for photoelectrochemical cells based on the n-CdS/S^{2-} system, but what matters is what happens to minority carriers *after* they have become trapped. According to Wilson,[44] oxidation of sulfide at n-CdS photoelectrodes is a two-step process:

$$h + S^{2-}_{ads} \rightarrow S^-_{ads} \quad (9a)$$

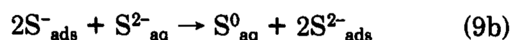

$$2S^-_{ads} + S^{2-}_{aq} \rightarrow S^0_{aq} + 2S^{2-}_{ads} \quad (9b)$$

The second step has to compete with the back-reaction

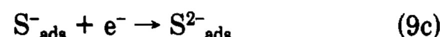

$$S^-_{ads} + e^- \rightarrow S^{2-}_{ads} \quad (9c)$$

Since the rate of reaction 9c depends on the supply of electrons, it becomes progressively smaller as the band bending is increased. Evenor et al.[40] have shown that high values of s_t are compatible with high photocurrent conversion efficiencies. Even though most holes are captured by surface states, reaction 9b competes so effectively with reaction 9c that efficient surface-mediated charge transfer occurs. The competition between these two routes has also been considered in detail by Li and Peter[45] for the more general case where the redox species are not adsorbed. Estimations of the interfacial reaction rate based on Marcus theory[5,46,47] suggest that effective mediated electron transfer will occur unless the reorganization energy of the redox reaction is very large. However, Li and Peter have pointed out that an important factor determining the competition between mediated transfer and recombination is the transmission factor for interfacial electron transfer. If the surface states are "buried" below a thin oxide layer or if they extend some way into the solid ("near surface states"[13,45]), then the transmission factor will be much less than unity and recombination will dominate.

Gmitter et al.[48] have used a contactless rf method to investigate the effects of Ru(III) adsorption[49-51] on surface recombination velocities for n-GaAs in selenide solutions. The technique was developed by Yablonovitch and co-workers,[52-54] who have applied it to a wide range of systems. Interestingly, the values of s_t for GaAs are much lower than those measured by Benjamin and Huppert[42] for CdS. For GaAs⟨100⟩ surfaces immersed in selenide/diselenide solution, s_t was found to be 1700 cm s^{-1}, whereas s_t for the etched starting surface in air was greater than 2×10^4 cm s^{-1}. In basic solutions, treatment of the GaAs surface with $RuCl_3$ increased s_t by more than 1 order of magnitude.

Time-resolved microwave conductivity measurements have also been used by Kunst et al.[55-59] to study excess charge carrier kinetics in different systems. Studies of undoped silicon[59] showed that the lowest surface recombination velocities were obtained for wafers treated with bichromate solution ($s_t < 10^3$ cm s^{-1}). Polishing the wafer was found to increase s_t to at least 10^6 cm s^{-1}. Extraordinarily low surface recombination velocities for silicon and germanium have been reported by Yablonovitch et al.[52] for wafers treated in HF solution; for Si⟨111⟩ $s_t = 0.25$ cm s^{-1}, and for Ge $s_t = 2$ cm s^{-1}. Interestingly, the photodissolution of silicon in this same electrolyte gives rise to photocurrent quadrupling at low light intensities,[30-32] and in situ infrared measurements[52,60] indicate that a hydrogenated silicon surface is formed under these conditions. This area is now expanding rapidly, largely as a result of the considerable interest in the reduction of surface recombination in GaAs solid-state devices by surface treatments, including dipping in sulfide solutions.[61,62]

B. Majority Carrier Capture by Surface States

The transfer and capture of carriers at the surface is evidently a fast process, but the photocurrent response contains another contribution. As minority carriers accumulate on surface states, the electron occupation factor (the quasi-Fermi level[5]) shifts away from its

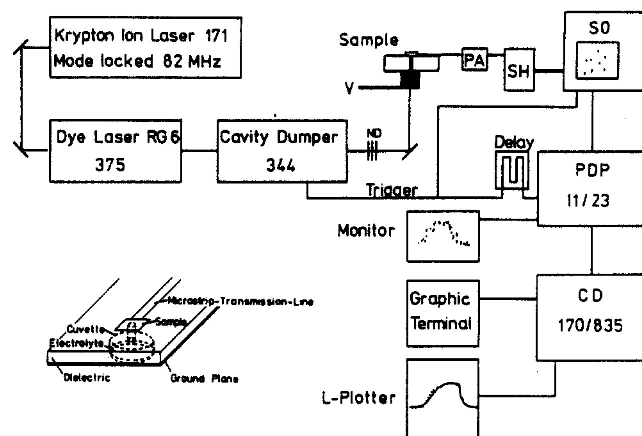

Figure 9. Apparatus for picosecond time-resolved photocurrent measurements: PA = preamplifier; SH = sampling head; SO = sampling oscilloscope; V = voltage supply; ND = neutral density filters. The inset shows the microstrip transmission line used to match the cell impedance (reproduced from ref 83; copyright 1986 Elsevier).

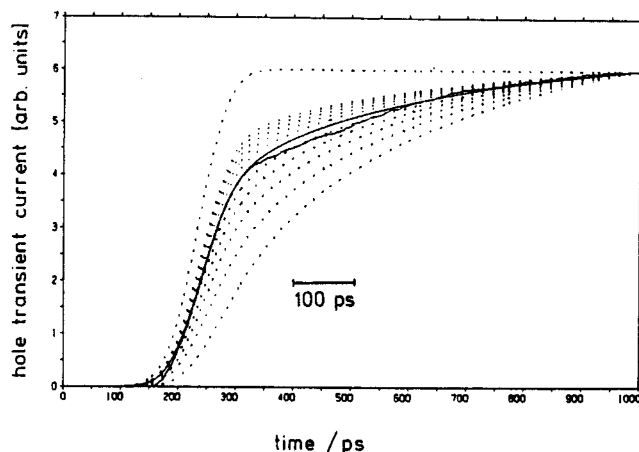

Figure 10. Transient response observed with the experimental arrangement in Figure 9 for illumination with a 20-ps (fwhm) laser pulse. Conditions: repetition rate, 5 kHz; wavelength, 594 nm; 10^8 photons/pulse. The wavy line is the experimental curve, and the drawn-out curve is the calculated response. The dotted lines are calculated for different relative contributions from the space charge and quasi-neutral regions corresponding to different values of the product αW (see ref 83 for details) (reproduced from ref 83; copyright 1986 Elsevier).

equilibrium value, and so majority carriers begin to flow into the surface where they annihilate the trapped minority carriers. Although this process is rapid close to flatband, it is generally much slower under depletion conditions since it depends on the concentration of majority carriers at the surface. If majority carrier transport through the space charge region is not rate-determining, the first-order rate constant k_r can be expressed in terms of the thermal velocity v and the capture cross section σ_r

$$k_r = v\sigma_r n_{surf} \tag{10a}$$

where n_{surf} the surface density of majority carriers can be calculated from the expression

$$n_{surf} = n_{bulk} \exp(-q\Delta\phi/kT) \tag{10b}$$

provided that illumination does not perturb the majority carrier Fermi level signficantly. Taking, for example, $e\Delta\phi = 0.2$ eV, $\sigma_r = 10^{-17}$ cm^2, $n_{bulk} = 10^{17}$ cm^{-3}, and $v = 10^7$ cm s^{-1}, we find $k_r = 3 \times 10^3$ s^{-1}; i.e., the surface states will require at about 1 ms to return to equilibrium after a light pulse, reflecting the low equilibrium concentration of majority carriers present at the surface under depletion conditions. By contrast, k_r at flatband is about 10^7 s^{-1}.

The collection of photogenerated carriers from the space charge and field-free regions has also been studied extensively by laser pulse induced photopotential and photocurrent transients.[63-87] These measurements are reviewed in more detail in section IV. Most of them are concerned with the decay part of the transient rather than the rising part containing information about carrier collection, but an exception is the particularly well-time-resolved study of minority carrier collection by Willig and co-workers,[83,85,86] who have used picosecond laser excitation to study the photocurrent response of the semiconductor electrolyte contact. By careful matching of the cell and circuit impedances, they have extended measurements into the subnanosecond region; the photoelectrochemical cell design and the associated instrumentation for picosecond resolved photocurrent measurements[83] are shown in Figure 9. The response to be expected for a defined laser pulse shape can be obtained from the time-dependent solution of the diffusion problem using standard Laplace transfor techniques,[86] and Figure 10 illustrates the excellent agreement between theory and experiment reported by Bitterling and Willig.[83]

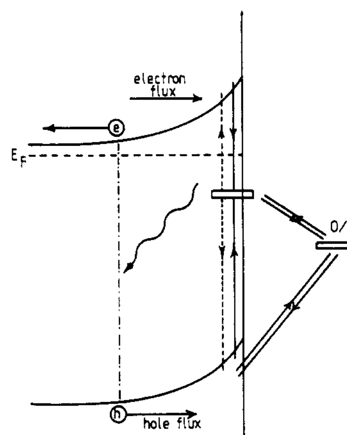

Figure 11. Routes for minority carrier reactions at the semiconductor electrolyte interface. The scheme shows direct transfer to redox species as well as indirect transfer via surface states, which competes with recombination. Note how the hole flux into surface states generates a coupled electron flux as the result of the recombination process. The net photocurrent is the sum of the hole and electron contributions.

The surface recombination velocity defined by eq 10 tells us nothing about the subsequent fate of trapped minority carriers, but this is exactly what interest us in the context of the photoelectrochemical reactions that occur at the semiconductor electrode. The possible reaction routes are illustrated in Figure 11.[3,15] For the present, we shall assume that recombination in the space charge region can be neglected so that minority carriers either recombine at the surface or are transferred to redox ions in the solution (reactions that involve multistep electron transfer or majority carrier injection are not considered in this scheme). An important point made by Figure 11 is that the oxidation of R may occur either directly by valence band holes or indirectly via holes trapped at surface states. Consequently, as discussed in the preceding section, high values of surface recombination velocity do not neces-

sarily imply low photocurrent conversion efficiencies; indeed, in many cases the converse is true.[41]

C. Generalized Treatment of the Non Steady State

Surface and bulk recombination processes have been treated extensively in the literature.[16-21,45] Full treatment of surface recombination for the non steady state[45] is beyond the scope of this review, and in order to simplify the discussion of the non-steady-state response of the semiconductor junction, a simpler, more "chemical" approach to the description of surface recombination will be pursued with the following scheme[3,88] for the case of an n-type semiconductor:

$$h\nu \rightarrow h + e^- \qquad (11a)$$

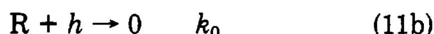

$$R + h \rightarrow 0 \quad k_0 \qquad (11b)$$

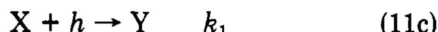

$$X + h \rightarrow Y \quad k_1 \qquad (11c)$$

$$Y + R \rightarrow X + 0 \quad k_2 \qquad (11d)$$

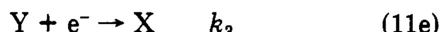

$$Y + e^- \rightarrow X \quad k_3 \qquad (11e)$$

Here k_0–k_3 are conveniently defined as pseudo-first-order rate constants; i.e., $k_0 = k_0'[R]$, $k_1 = k_1'[X]$, $k_2 = k_2'[R]$, and $k_3 = k_3'[e^-]$.

The surface concentration of X in this scheme represents the density of surface states that are occupied by majority carriers and are therefore able to capture minority carriers. The fraction of occupied states is potential dependent since it is determined by the position of the Fermi level with respect to the energy level of the surface state. It follows that the surface concentration of Y represents the density of states that are effectively "occupied" by holes. The capture of holes by the surface states X can be considered for the limiting case of small perturbations under conditions where thermal release of carriers is negligible. In fact, the problem can be solved without making these assumptions,[45] but for the present purposes it is more convenient to use the simple "irreversible" scheme since it allows straightforward derivation of the time-dependent response. It can be seen from the reaction scheme that recombination involves sequentially capture of a hole by X followed by capture of an electron by Y, and it follows that the flux of holes into the surface states generates a corresponding electron flux. Surface-mediated electron transfer, on the other hand, corresponds to reaction 11c followed by reaction 11d.

The first-order reaction scheme in eq 11 can be used to derive the response of the system to any form of optical perturbation.[3] The total time-dependent photocurrent in the external circuit originates from two contributions:

$$j_{photo}(t) = j_{hole}(t) + j_{electron}(t) \qquad (12)$$

It is convenient to assume that the excitation gives rise to an instantaneous flux of minority carriers $j_{hole}(t) = g(t)$ (given by eq 2) into the interface. This assumption is satisfactory provided that the transit and diffusion times are small compared with the time scale of the experiment (this point was discussed originally by Gärtner[10]). Under these conditions, j_{hole}, the minority carrier flux, follows the excitation profile. By contrast, $j_{electron}$ will lag behind j_{hole} since the electron flux is responding to the changes in surface-state population.

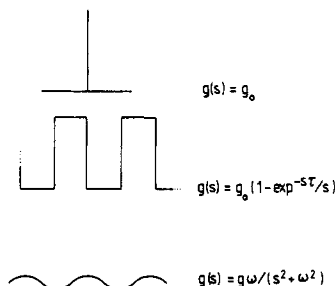

Figure 12. Three profiles used for optical excitation of semiconductor electrodes. The Laplace transforms of the time-dependent functions are also shown. These are used to derive the photocurrent response from the interfacial transfer function.

At this point it would be possible to consider a range of different excitation profiles—laser flash, chopped illumination, and so on—in order to obtain exact expressions for eq 12. However, all forms of excitation can be allowed for by adopting a more general approach.[3] Standard Laplace transform methods can be applied to the set of first-order differential equations derived from eq 11 to obtain the *interfacial transfer function* $T_1(s)$ in terms of the rate constants (s is the Laplace variable):

$$T_1(s) = \mathcal{L}j_{photo}(t)/\mathcal{L}g(t) = \bar{j}_{photo}(s)/\bar{g}(s) \qquad (13)$$

The net carrier flux at the interface for any form of excitation can be derived from eq 13 by substituting for the appropriate transform $\bar{g}(s)$ of the excitation function. The excitation profiles of practical importance are shown along with their transforms in Figure 12.[3]

The situation is not quite so simple, however, because the photocurrent response observed experimentally is determined not only by the factors discussed above but also by the transfer function of the cell $T_c(s)$. If the impedance of the counter electrode is negligible or if potentiostatic control is applied, the cell-transfer function is determined only by the space charge capacitance and the solution resistance. The transform T_t of the total response can therefore be expressed as the product

$$T_t(s) = T_i(s)\ T_c(s) \qquad (14a)$$

where the transfer function $T_c(s)$ is given by

$$T_c(s) = \tau_{RC}^{-1}/(s + \tau_{RC}^{-1}) \qquad (14b)$$

Here $\tau_{RC}^{-1} = R_{sol}C_{sc}$. If an external measuring resistor R_m is used to measure the photocurrent, R_{sol} is replaced by $R_{sol} + R_m$.

IV. Laser-Induced Photocurrent Transients

The approach outlined in the preceding section is relevant to the extensive literature on laser-induced photocurrent transients.[63-87] Although more detailed treatments consider the shape of the excitation pulse,[85] it is convenient for the sake of clarity to assume that the exciting flash is sufficiently short to produce a minority carrier flux into the interface that approximates the δ function. If there are no recombination losses, the separation of holes and electrons simply charges the space charge capacitance C_{sc}, which subsequently discharges through the solution resistance R_{sol} and the measuring resistor R_m. In the absence of surface recombination, the current decays exponentially

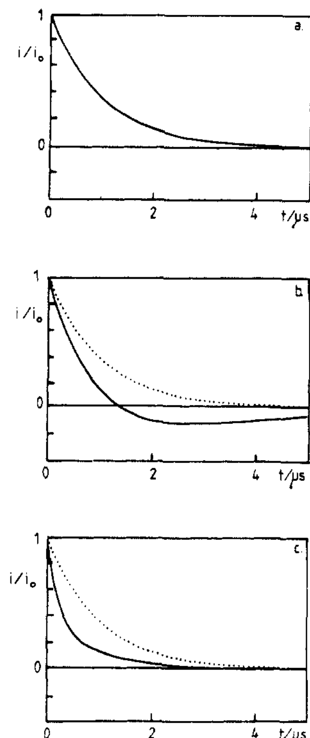

Figure 13. Photocurrent transient response to a δ function excitation (short laser pulse) calculated from the reaction scheme shown in eq 11. The RC time constant of the cell and measuring resistor is 1 μs. Key: (a) no surface recombination; (b) $k_1 = k_2$, $k_3 = 5 \times 10^5$ s^{-1}; (c) $k_1 = k_2$, $k_3 = 2 \times 10^6$ s^{-1}. Note that the photocurrent only overshoots as in b when recombination is slow compared with the RC time constant. If recombination is rapid, as in c, the photocurrent decays more rapidly than the RC limit but does not overshoot.

with a time constant given by the product $C_{sc}(R_{sol} + R_m)$. It is clear that no information about rate processes is available from the decay of the photocurrent in this case. If minority carriers are trapped at the surface, however, the photocurrent transient also contains a contribution from the majority carrier flux induced by recombination.

The transients shown in Figure 13 illustrate the important features of the calculated response[3] (refer to eq 11 for definition of the rate constants). In the absence of surface recombination, the photocurrent decays with a time constant determined by the product $C_{sc}(R_{sol} + R_m)$ (Figure 13a). If recombination is relatively slow ($k_3^{-1} > (R_{sol} + R_m)C_{sc}$), the majority carrier flux causes the photocurrent to overshoot (Figure 13b). If, on the other hand, recombination is fast ($k_3^{-1} < C_{sc}(R_{sol} + R_m)$), the majority carrier flux causes the photocurrent to decay *more rapidly* than expected from the $(R_{sol} + R_m)C_{sc}$ time constant, as shown in Figure 13c.

Before the theoretical response is compared with experimental data, it is necessary to identify conditions under which more complicated photocurrent transients are to be expected. First, the derivation assumes that the perturbation is sufficiently small that second-order recombination processes are unimportant. This can be a serious problem since the majority of experimental studies have used high-power laser excitation. It is therefore important to establish that measurements are performed in the linear regime, and it is also preferable to measure the quantum efficiency. Second, multistep electron-transfer reactions such as photodecomposition, oxygen evolution, or current doubling will give more

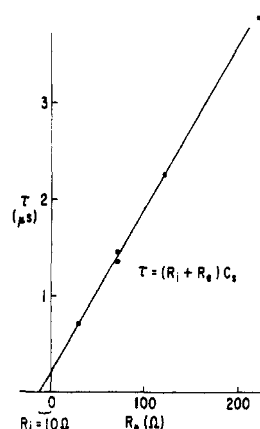

Figure 14. Experimental determination of the solution cell resistance (R_i) from the decay time constant measured for n-CdSe in 1 M KCl with different load resistors (R_1) (reproduced from ref 78; copyright 1985 The Electrochemical Society).

complicated rate expressions involving the surface concentration of intermediates (the special case of current multiplication reactions is considered later in this review). Third, if there is appreciable trapping of carriers in the space charge region, the rise time of the photocurrent may be increased.[41] This is likely to be a problem in polycrystalline or amorphous semiconductor electrodes. Last, it is assumed that the space charge capacitance in the semiconductor is much smaller than the Helmholtz capacitance[5] and that the amount of charge accumulating at the surface is insufficient to change the potential drop in the Helmholtz layer.

In the absence of recombination, the photocurrent transient is determined only by the time constant $\tau_{RC} = (R_{sol} + R_m)C_{sc}$ so that the potential dependence of the decay rate simply reflects the change in space charge capacitance. The linear dependence of τ on R_m is usually checked by varying R_m; an example of the application of this procedure to photocurrent transients measured at CdSe by Wilson et al.[78] is given in Figure 14, which shows how the value of R_{sol} is obtained from the intercept of the plot.

τ also depends on the value of C_{sc}, which can therefore be determined if R_{sol} is known. The space charge capacitance of a uniformly doped semiconductor under depletion conditions is described by the *Mott-Schottky equation*[5]

$$C_{sc}^{-2} = (2/qN\epsilon\epsilon_0)(\Delta\phi - kT/q) \qquad (15)$$

Plots of C_{sc}^{-2} vs potential are commonly used to evaluate flatband potentials and doping densities. If recombination is unimportant, then plots of τ^2 vs potential should also be linear. This kind of behavior has been reported by Wilson et al.[78] for CdSe in KI and KCl and by Sakata et al.[84] for WSe_2. Examples of the photocurrent transients obtained by Sakata et al. are shown in semilogarithmic form in Figure 15a, and the corresponding linear plots of τ^2 against potential are shown in Figure 15b.

Although Sakata et al. were able to show that plots of τ^{-2} against potential were linear as expected if the space charge capacitance follows the Mott-Schottky equation, they also found that transients measured close to the flatband potential displayed an initial fast component that was clearly decayed more rapidly than $(R_{sol} + R_m)C_{sc}$. This result, which is shown in Figure 16 can

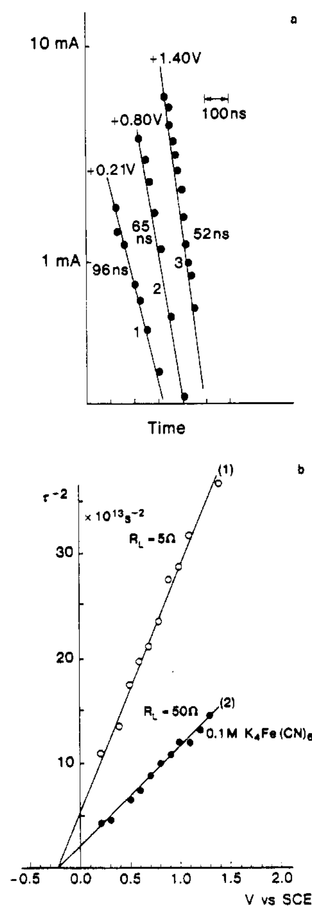

Figure 15. (a) Semilogarithmic plots used to obtain the dependence of photocurrent decay time on electrode potential (vs SCE) for n-WSe_2 in 0.1 M $K_4Fe(CN)_6$/0.1 M $K_3Fe(CN)_6$. (b) Plots of τ^{-2} vs potential (corresponding to Mott-Schottky plots of C_{sc}^{-2} vs potential) for n-WSe_2 in 0.1 M $K_4Fe(CN)_6$/0.1 M $K_3Fe(CN)_6$ for two different values of the load resistor, R_L (reproduced from ref 84; copyright 1986 The Electrochemical Society).

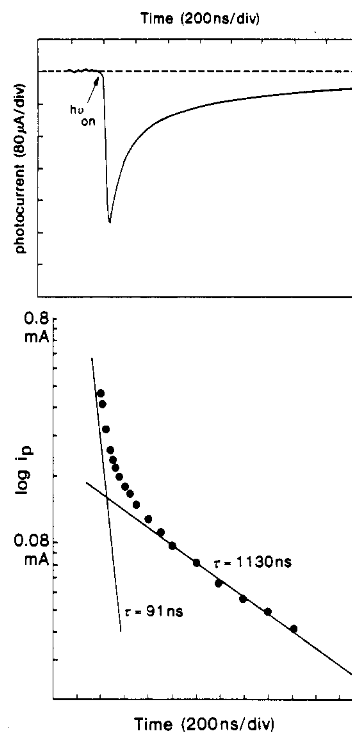

Figure 16. Photocurrent transient and corresponding semilogarithmic plot for n-WSe_2 in 1.0 M KI at −0.30 V vs SCE showing the rapid-decay component at short times that can be attributed to recombination (compare Figure 13c) (reproduced from ref 84; copyright 1986 The Electrochemical Society).

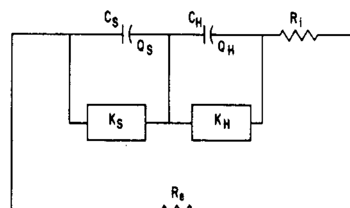

Figure 17. Equivalent circuit proposed by Wilson et al.[78] to describe the transient photocurrent behavior of the semiconductor/electrolyte interface. C_s and C_H are the space charge and Helmholtz capacitances. R_l is the solution resistance, and R_1 is the external load. K_s and K_H are first-order rate constants describing charge transfer across the interface (reproduced from ref 78; copyright 1985 The Electrochemical Society).

be explained by the fact that $(R_{sol} + R_m)C_{sc}$ increases as the potential approaches flatband, whereas the time constant for recombination becomes smaller because more majority carriers are available. Close to flatband, the recombination time constant becomes shorter than $(R_{sol} + R_m)C_{sc}$ and the transient decay is faster since it contains the fast majority carrier component. Application of this analysis to the experimental data shown in Figure 16 gives a value of about 10^7 s^{-1} for the rate constant for majority carrier capture by surface states.

By contrast, transients showing the overshoot characteristic of slow recombination can be found in many papers, including, for example, the work of Wilson et al. on CdSe,[78] Cook et al.[81] on p-Inp, and Jaegermann et al.[77] on n-PtS_2. The overshoot is explained adequately by the simple scheme outlined above, but a different approach should also be mentioned. Wilson et al.[78] have proposed the equivalent circuit shown in Figure 17 to describe the time dependence of recombination and charge transfer to solution redox species, and an essentially identical circuit has been discussed by Willig.[86] k_s and k_H (which are represented by equivalent current generators in Willig's circuit) represent rate constants for recombination and interfacial electron transfer, respectively. They can be identified with k_3 and k_0 in eq 11. It is doubtful, however, whether these equivalent circuits give any better insight into the physical processes involved since the recombination time constant cannot be represented by a physically meaningful RC combination.

Since the dominant factor in the transient decay is the time constant $(R_{sol} + R_m)C_{sc}$, care is needed in the interpretation of the effects of changing the solution composition or of modifying the electrode surface. It will generally be necessary to measure the capacitance voltage behavior of the system, preferably under illumination, in order to detect shifts in the flatband potential. If this is not done, changes in the decay rate constants may be incorrectly attributed to kinetic effects when in fact they arise from changes in the space charge capacitance at a given potential. It should be mentioned, however, that several authors have dissented from the view that the RC time constant dominates the transient photocurrent response. Prybyla et al.,[75] for example, concluded from a detailed study of transient photocurrents at WSe_2 and $MoSe_2$ electrodes that other effects must be important since the transients decayed faster than expected from the RC time constant. This could, however, have been the result of recombination effects.

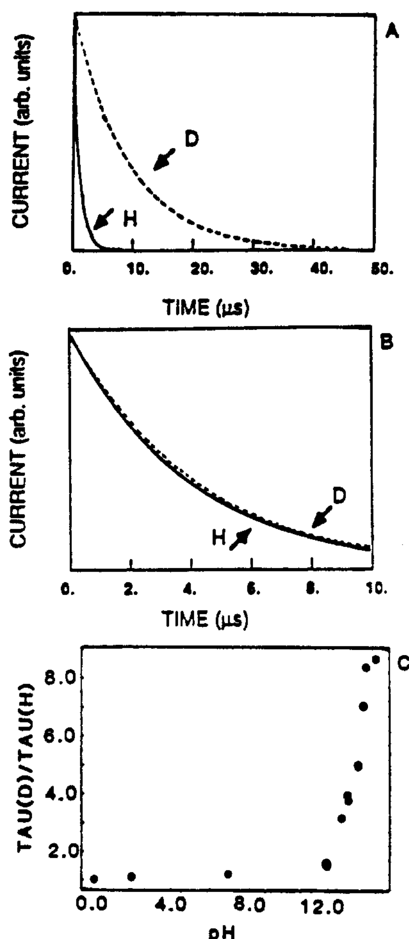

Figure 18. Photocurrent transients for the photooxidation of water at n-TiO_2 showing (A) the large effect of replacing 1 M $NaOH/H_2O$ with 1 M $NaOD/D_2O$, (B) no isotope effect when 1 M H_2SO_4/H_2O is replaced by 1 M D_2SO_4/D_2O, and (C) the pH dependence of the isotope effect (reproduced from ref 87; copyright 1989 American Chemical Society).

It might seem from the preceding discussion that there is little convincing evidence that the rates of interfacial electron transfer are accessible from transient photocurrent measurements. However, this view contradicts the conclusion reached by Cook et al.,[82] who maintain that the decay time constant measured at p-InP modified by metal deposition contains information about the faradaic resistance R_F for the evolution of hydrogen (R_F is defined as RT/nFi_0, where i_0 is the exchange current density). These authors assume that $\tau = (R_{sol} + R_m + R_F)C_{sc}$ and interpret their results using a conventional resistive equivalent circuit to represent the semiconductor/electrolyte junction. It is not clear, however, whether the concept of the faradaic impedance can be applied in this way to the minority carrier reactions occurring far from equilibrium. Norton et al.[87] also present convincing evidence that photocurrent transients contain kinetic information about charge transfer. In a study of the n-TiO_2/solution interface, these authors found a pronounced H/D isotope effect in alkaline but not in acid solutions; their transients are shown in Figure 18. The decay time constants are rather slow (of the order of 10 μs), but this probably reflects the fact that highly doped TiO_2 was used ($N_d = 10^{19}$ cm^{-3}). These results certainly suggest that kinetic information is indeed contained in the decay behavior associated with multistep electron-transfer reactions. It is clear, nevertheless, that some aspects of

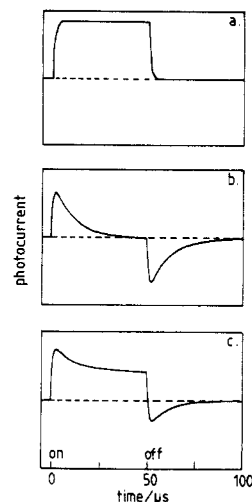

Figure 19. Transient photocurrent response to chopped illumination calculated for the reaction scheme in eq 11 ($R_{sol}C_{sc} = 10^{-6}$ s): (a) no recombination; (b) almost complete recombination ($k_2 \gg k_1$, $k_3 = 10^5$ s^{-1}); (c) partial recombination ($k_1 = k_2$; $k_3 = 10^5$ s^{-1}). The calculated transients can be compared with the experimental transient for p-GaP shown in Figure 20.

the interpretation of photocurrent transients still remain controversial after nearly a decade of investigation, and there is plenty of scope for further work, particularly on multistep photoelectrode reactions.

Finally, the work of Fichou, Frippiat, Kirsche de Mesmaeker, and co-workers[89-93] should be mentioned in which the laser pulse is used to excite an adsorbed dye that then takes part in an electron-transfer process. These reactions are complicated, and their discussion lies outside the scope of this review, but non-steady-state measurements have made a major contribution in this interesting area.

V. Photocurrent Response to Chopped Illumination

Photocurrents at semiconductor electrodes are often measured by interrupting the illumination with a rotating segment chopper so that a lock-in amplifier can be used to discriminate against background currents. At potentials sufficiently far from flatband, the photocurrent response usually follows the illumination profile, but close to flatband relaxation effects are commonly observed, giving rise to attenuation and phase shift in phase-sensitive lock-in measurements. These effects are characteristic of surface recombination, and they arise from the fact that the electron and hole currents have different relaxation times and opposite signs.[94,95]

The time-dependent photocurrent response to chopped illumination is obtained by substituting the transform of the square-wave input function into eq 14 followed by inverting the resulting output transform.[3] The main features of the photocurrent transients expected for different cases are illustrated in Figure 19. The calculations show that the rise time of the current is determined by $R_{sol}C_{sc}$ (it is assumed that R_m is zero under potentiostatic conditions), whereas the subsequent decay is determined by the rate at which minority carriers trapped at surface states capture majority carriers. At long times, the photocurrent approaches a steady-state value that depends on the *relative* rates of recombination and charge transfer to redox species.

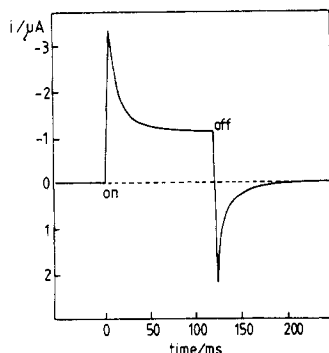

Figure 20. Photocurrent transient observed for p-GaP in 0.5 M H_2SO_4 at 0.225 V vs SCE, showing the decay and overshoot characteristic of surface recombination. In this case the recombination centers have been identified as hydrogen atoms that diffuse into the near-surface region.

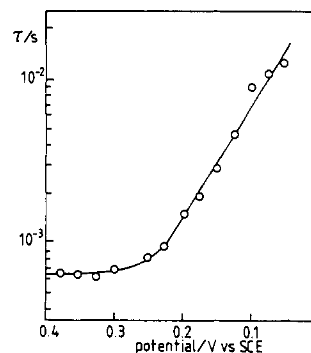

Figure 21. Potential dependence of the decay time constant for p-GaP in 0.5 M H_2SO_4. Note in particular that τ becomes independent of potential at potentials more positive than 0.25 V, indicating that the band bending no longer changes with potential ("Fermi level pinning").

When the light is interrupted, the carriers trapped on surface states still continue to recombine, and so the current changes sign since it is now only due to the majority carriers flowing to surface states. As the remaining trapped carriers recombine, the "overshoot" current decays with the same time constant as that observed during the on period.

An experimental example of the kind of transient response discussed above is shown in Figure 20 for p-GaP in acid solution.[13] The photocurrent decays exponentially toward a steady-state cathodic value after the light is switched on and then overshoots to give an anodic transient when the light is switched off. Since we are dealing with a p-type semiconductor, surface recombination involves the capture of photogenerated electrons at surface states followed by the influx of holes. In this particular case, it has been shown that the surface states are formed under illumination as the result of the photogeneration of hydrogen atoms diffusing into the semiconductor surface.[13] The recombination reaction then involves electron capture by H^+ ions in the lattice, which act as "near-surface" states, and subsequent capture of a hole by the hydrogen atom. Surface states that are located close to but not actually at the surface are particularly effective for recombination since the tunneling probability for electron transfer to solution redox species is small.[45]

The recombination reaction can be represented by the sequence

$$h\nu \rightarrow h + e^- \quad (16a)$$

$$H^+_{nss} + e^- \rightarrow H^\bullet_{nss} \qquad k_1 \quad (16b)$$

$$H^\bullet_{nss} + h \rightarrow H^+_{nss} \qquad k_3 \quad (16c)$$

(compare eq 11 for the definition of the pseudo-first-order rate constants).

If we assume that the equilibrium hole density is essentially unperturbed by illumination, then the surface density of majority carriers (holes in this case) is related to the band bending (in the Boltzmann limit) by eq 10b. As a consequence, the first-order rate constant k_3 $(=k_3'[h])$ in eq 16c should vary by a factor of 10 for a potential change of 59 mV. In fact, this "Nernstian" behavior is not observed experimentally in the case of p-GaP; instead, as Figure 21 shows, a semilogarithmic plot of the decay time constant against electrode potential has a slope of 120 mV per decade over most of its length. Close to the flatband potential, on the other hand, the decay time constant appears to approach a constant value.

The simplest explanation of the behavior shown in Figure 21 is that not all of the change in applied potential appears across the space charge region. There are two possible reasons for this. The first is that the charge stored in surface states varies with potential, giving rise to a surface-state capacitance so that the potential distribution across the semiconductor/electrolyte junction varies with applied potential as the occupancy of the surface states changes. The variation ΔV in the potential drop across the electrical double layer on the solution side (the Helmholtz layer) potential is given by

$$\Delta V = qN_s f_s / C_H \quad (17)$$

where C_H is the capacitance of the Helmholtz layer, N_s is the density of surface states, and f_s is their occupancy factor. A high density of surface states is needed to produce an appreciable change in potential; 10^{13} states cm^{-2}, for example, give a maximum change of about 100 mV. Under extreme conditions ($N_s > 10^{14}$ cm^{-2}), virtually all of the change in potential appears across the Helmholtz layer as the result of surface charging, and the band bending in the semiconductor remains constant. This effect has been described as *Fermi-level pinning*[8] by analogy with the behavior of solid-state contacts. However, it is important to realize that the "surface states" at the semiconductor/electrolyte interface are not necessarily an intrinsic property of the junction arising from "dangling bonds" but are more likely to arise as the result of interfacial chemistry such as photocorrosion. Consequently, the density of surface states will depend in most cases on potential and illumination level.

The second possible explanation for the sub-Nernstian potential dependence of surface state relaxation is that the composition or degree of oxidation of the semiconductor surface varies with potential. The potential distribution is sensitive not only to the electronic charge but also to ionic and dipole contributions. In many cases, the flatband potential shows a Nernstian dependence on pH as the result of the dissociation of surface groups,[5] and shifts due to anion adsorption, e.g., HS^- on CdS, are also observed.[96] These results point to a strong interaction of the semiconductor with the solution, and it seems probable that the surface atoms of the semiconductor are chemically bonded to form, for example, –OH and –H species. If the surface com-

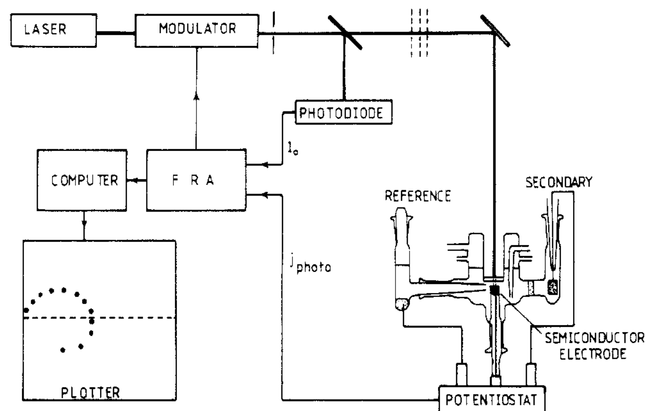

Figure 22. Experimental arrangement for intensity-modulated photocurrent spectroscopy (IMPS). The frequency response analyzer (FRA) measures the complex ratio of the ac photocurrent to the ac illumination signal.

position of the semiconductor changes with potential, then the surface dipole will not be constant; i.e., the band edges are not pinned at a fixed energy but move instead as the potential changes.

Relaxation effects have been observed in the photocurrent response of other systems,[97-101] with time constants ranging from milliseconds (for example in the case of anodic oxide films on iron[94]) to seconds (in the case of TiO).[99-101] The simple recombination scheme discussed here may not be appropriate for all systems, particularly if multistep electron-transfer reactions are involved.

VI. Intensity-Modulated Photocurrent Spectroscopy

The optical perturbations discussed so far have electrical analogues that are widely used in electrochemistry. Thus, the laser pulse technique corresponds to the coulostatic method, where a short current pulse is used to inject charge into the metal solution interface; chopped illumination, on the other hand, is closely related to the current step or galvanostatic technique. This analogy can be extended to ac impedance techniques involving sinusoidal modulation of current or potential, which have found widespread application in electrochemistry. The corresponding sinusoidal optical excitation can be generated by using an acoustooptic modulator to produce sinusoidal modulation of a laser beam[102-106] or, over a more restricted frequency range, by modulation of the output of an arc lamp.[97,107] The time-dependent incident illumination is therefore of the form

$$I(t) = I_0(1 + \delta \sin(\omega t)) \qquad (18)$$

where δ is the depth of modulation and I_0 is the mean intensity.

In the technique known as *intensity-modulated photocurrent spectroscopy* (*IMPS*), the complex ratio of photocurrent flux to incident light flux is measured over many decades of frequency with a frequency response analyzer. The experimental arrangement is shown in Figure 22.

If surface recombination occurs at an illuminated semiconductor electrode, the response to intensity-modulated illumination will be made up of two components associated first with the photogenerated minority carriers and second with the majority carriers

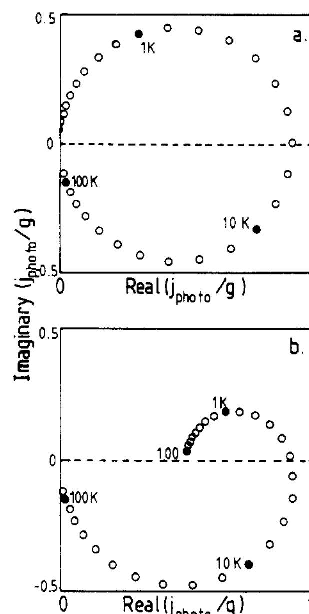

Figure 23. Theoretical IMPS plots calculated from the reaction scheme in eq 11 ($R_{sol}C_{sc} = 10^{-5}$ s): (a) almost complete recombination, $k_2 \gg k_1$, $k_3 = 10^4$ s^{-1}; (b) partial recombination, $k_1 = k_2$, $k_3 = 10^4$ s^{-1}. The upper semicircle is determined by recombination ($\omega_{max} = k_3$) and the lower circle by the cell time constant ($\omega_{min} = (R_{sol}C_{sc})^{-1}$).

that must flow to the surface in order to take part in surface recombination. The two currents have opposite signs of course, and generally they will not be in phase. As a consequence, both the phase and magnitude of the net photocurrent will vary with frequency in a way that is related to the kinetics of recombination.

The IMPS response of the semiconductor/electrolyte interface has been discussed in detail elsewhere.[3,103,88] The solution to the kinetic scheme involves substitution into eq 14 of the tranform appropriate for a sinusoidal excitation signal to obtain the transform of the output photocurrent. Inversion then leads an expression for the complex ratio j_{photo}/g of the form

$$j_{photo}(\omega)/g(\omega) = \mathrm{Real}(j_{photo}(\omega)/g(\omega)) + \mathrm{Imag}(j_{photo}(\omega)/g(\omega)) \qquad (19)$$

where $g(\omega)$ is the periodic flux of photogenerated carriers corresponding to the Gärtner equation. The ratio $j_{photo}(\omega)/g(\omega)$ is the ac analogue of the quantum efficiency. It can be represented as a complex number since it is effectively a gain factor that has both phase and magnitude.

The frequency dependence of the normalized photocurrent can be examined most conveniently by plotting it in the complex plane. The resulting plots should not be confused with impedance diagrams; they actually represent the dimensionless "complex gain" of the photoelectrode. The most interesting feature of the response is that it extends into two quadrants of the complex plane since the phase shifts associated with the effects of recombination and of $R_{sol}C_{sc}$ have opposite signs. This may appear odd at first sight, but the majority carrier current only appears to lead rather than lag behind the excitation because it has the opposite sign to the minority carrier current.

The predicted IMPS response can be illustrated by considering some special cases illustrated in Figure 23. If there is no surface recombination, the photocurrent follows the illumination exactly at low frequencies and

the photocurrent conversion efficiency is given by the Gärtner equation. Since the plots are normalized, this means that the low-frequency intercept occurs at unity. As the frequency is increased, the effects of the $R_{sol}C_{sc}$ time constant become evident and the photocurrent is attenuated. The frequency response traces out a semicircle in the lower quadrant of the complex plane, with the lowest point occurring at a frequency of $(2\pi R_{sol}C_{sc})^{-1}$.

If, at the other extreme, recombination is very effective, most of the photoexcited carriers fail to cross the interface. Instead, they are trapped by surface states and are annihilated subsequently by majority carriers. Under steady-state conditions, the photocurrent conversion efficiency is very small. The situation is different, however, when the illumination is modulated in intensity. Now the majority carrier current is attenuated as the frequency is increased because the kinetics are fairly slow under depletion conditions (i.e., $\omega > k_3$ in eq 11). At sufficiently high frequencies, the recombination is effectively "frozen out" and the ac photocurrent conversion efficiency approaches the Gärtner limit; i.e., the ratio j_{photo}/g tends toward unity on the real axis. At higher frequencies, however, the ac photocurrent is attenuated by the $R_{sol}C_{sc}$ time constant. These two effects combine to give a frequency response of the photocurrent tracing out a full circle that starts at the real axis, moves through the upper and lower quadrants, and tends toward the origin at high frequencies. The time constant associated with the recombination process (effectively $(k_3 + k_4)^{-1}$ in eq 11) can be calculated from the frequency ω_{max} at which the maximum in the upper quadrant of the complex plane occurs. The corresponding decay time constant observed with chopped illumination is $\tau = \omega_{max}^{-1}$.

In general, the predicted IMPS response will lie between the two limiting cases outlined above, and it contains a great deal of information that can only be resolved adequately by analysis in the frequency domain. The low-frequency intercept will occur at a nonzero value corresponding to the steady-state photocurrent, giving a measure of the relative rates of charge transfer and recombination (see Figure 23b). Unfortunately, however, the analysis shows that the absolute rates of minority carrier reactions are not directly accessible. Since it depends in part on the rate of minority carrier transfer across the interface, the low-frequency intercept is expected to vary with the concentration of redox species. The recombination time constant can be derived from the maximum in the upper quadrant, provided that it is considerably larger than $R_{sol}C_{sc}$, and it will also depend on the concentration of redox species if electron exchange via surface states is possible. The response in the lower quadrant can be analyzed to determine C_{sc} if R_{sol} is known.

The predicted trends in IMPS response have been confirmed by Peat and Peter[110] in a study of the anodic oxide film on iron, where the effects of adding ferrocyanide as an electron donor were investigated. Figure 24 shows a set of experimental IMPS plots for the passive film obtained for successive additions of $K_4Fe(CN)_6$ to the solution. The plots illustrate the transition from complete recombination control (circular plot) to recombination-free behavior (semicircle only in the lower quadrant). The well-developed semicircle in the lower quadrant is due to the fact that the capacitance of the thin oxide film is much higher than C_{sc} for most semiconductors. The analysis of the dependence of ω_{max} on ferrocyanide concentration proved that surface-mediated charge transfer does not occur in this system.

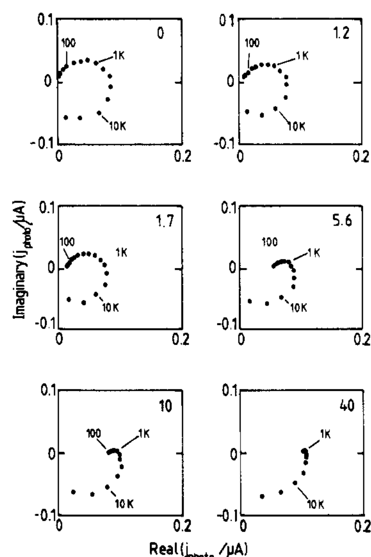

Figure 24. Experimental IMPS plots measured at a passive iron electrode in 0.1 M KOH at 0.5 V vs Hg/HgO, showing the effect of successive additions of $K_4Fe(CN)_6$. The concentrations are shown in millimolar. In the absence of ferrocyanide, recombination is almost complete (no steady-state photocurrent), whereas the addition of 40 mM ferrocyanide suffices to suppress recombination entirely. The result show that $Fe(CN)_6^{4-}$ is oxidized by valence band holes but not via surface states.

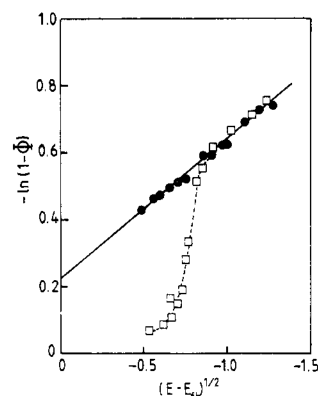

Figure 25. Determination of the electron diffusion length in p-GaP from the high-frequency IMPS limit ($j_{photo}/g \rightarrow 1$; closed circles). The plot also shows that the data obtained from the low-frequency intercept (open squares) deviate from the ideal line as the result of surface recombination.

One interesting feature of the IMPS method is that it can be used to effectively "freeze-out" the recombination effects, which causes problems when the minority carrier diffusion length is determined from the Gärtner equation. The photocurrent corresponding to the high-frequency intercept on the real axis is used instead of the steady-state photocurrent to construct plots similar to those shown in Figure 3. This method has been applied by Peat and Peter[14] to determine the electron diffusion length in p-GaP, and Figure 25 illustrates the improvement in the analysis that can be achieved in this way.

It is interesting at this point to relate the IMPS response to the transient response to interrupted illumination. Figure 26 is a set of experimental IMPS plots

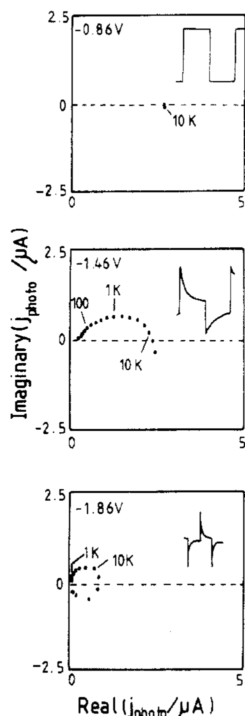

Figure 26. Comparison of IMPS and square-wave-modulated photocurrent responses for n-GaAs in 0.1 M KOH/14 mM K_2Se at different potentials (vs SCE). The square-wave frequency is 250 Hz in the upper two plots and 1 kHz in the lower plot. The plots illustrate the transition from recombination free response at −0.86 V to complete recombination at −1.86 V (close to E_{fb}).

obtained for n-GaAs in alkaline selenide solution.[15] The transient response is also shown in each case. In the saturation photocurrent region, the IMPS response is restricted to a point on the real axis corresponding to the Gärtner flux since no recombination occurs. The corresponding transient response is in phase with the illumination and shows no relaxation or overshoot. As the potential is made progressively more negative, the effects of surface recombination become more evident as a semicircle in the upper IMPS plane and as relaxation and overshoot in the transient response. Close to the flatband potential, recombination is complete; the IMPS response collapses to a circle, and symmetrical anodic and cathodic photocurrent transients are observed.

The IMPS technique is very sensitive to changes in the potential distribution at the semiconductor solution interface since it measures the rate of recombination. The variation of the recombination rate with potential has been discussed in the previous section, where it was shown that the ideal "Nernstian" dependence was not observed in the case of p-GaP in acid solution. A more extreme example of the sensitivity of the method is given in Figure 27, which shows the potential dependence of the recombination time constant for n-GaAs in alkaline selenide solution. Instead of the expected monotonic increase of τ with applied potential, the experimental data for the unmodified electrode reveal that τ actually *decreases* with potential over a region of about 300 mV. This extraordinary result indicates that the band bending decreases with increasing potential in this region as the result of changes in surface composition brought about by photocorrosion (similar results have also been obtained for n-GaAs in polysulfide solution[104]). Interestingly, ruthenium treatment

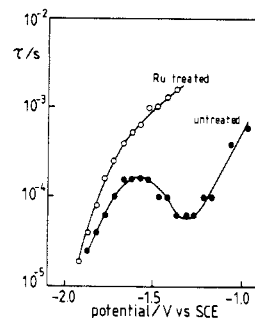

Figure 27. Potential dependence of the recombination time constant $\tau = \omega_{max}^{-1}$ for n-GaAs in 0.1 M KOH/14 mM K_2Se. The untreated GaAs exhibits very nonideal behavior (evident also in the photocurrent–voltage curves in Figure 5b), whereas the ruthenium-treated surface approaches ideal junction behavior more closely. The results suggest that adsorbed Ru acts as a mediator for hole transfer, preventing photocorrosion of the surface.

of the n-GaAs electrode stabilizes it so that the potential dependence of the recombination time constant becomes monotonic as shown in Figure 27.

It has been assumed in the preceding discussion that the semiconductor surface is homogeneous and adequately characterized by a uniform distribution of surface states. This is almost certainly an oversimplification since it is reasonable to suppose that surface states are associated with regions of physical or chemical inhomogeneity on the surface. Consequently, the potential distribution must be considered as a three-dimensional problem, and in the limit that surface features such as steps or patches of oxide are more widely spaced than the Debye length of the semiconductor, they will give rise to a lateral variation of band bending and of majority carrier concentration so that the time constant for recombination depends on position. If a Gaussian distribution of surface potential exists about some mean value, the semicircular IMPS response will be flattened.[104] If, on the other hand, the surface consists of patches of oxide, the potential distribution will be centered on two different values corresponding to bare and oxide-covered areas and the IMPS response will show two overlapping semicircles in the upper quadrant.[104] Examples of the effects of surface heterogeneity on the IMPS response have been observed for n-GaAs in alkaline solution[104] and for n-Si in fluoride solution[32,108] (see also section VII).

VII. Non-Steady-State Analysis of Photocurrent Multiplication

The phenomenon of photocurrent multiplication has already been discussed in section II.C. These reactions present an exciting challenge, but there have been few attempts to use non-steady-state methods to deconvolute the steps involved. Cardon and Gomes[108,109] appear to have been the first to realize that it should be possible to measure the rate constants for majority carrier injection by measuring the noise spectrum because minority carrier capture and majority carrier injection are correlated events, separated by a delay characteristic of the lifetime of the intermediate. In the case of current doubling on ZnO, these authors concluded that electron injection must occur in less than 10^{-4} s, which represented the limit of time resolution available in their measurements. More recently IMPS has been used to study current-doubling and current-quadrupling

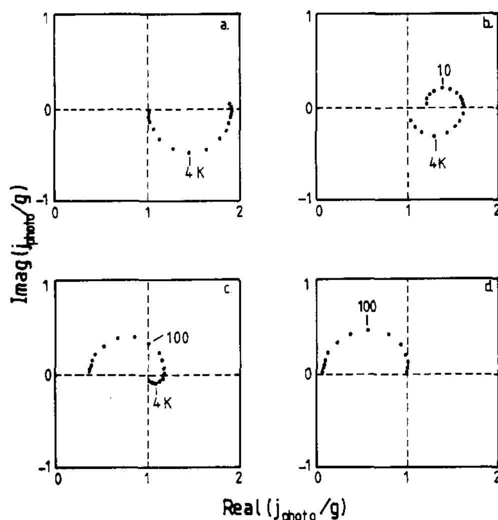

Figure 28. Theoretical IMPS plots for current doubling calculated from the reaction scheme in eq 20, showing the transition from current doubling control to recombination control (surface-state density 10^{12} cm^{-2}) as the band bending is decreased from (a) 0.45 V to (d) 0.3 V. The rate constant for hole injection, k_i, was taken as 2.5×10^4 s^{-1}.

reactions,[32-34] and in these cases majority carrier injection was found to be sufficiently slow to be accessible to measurement.

Current doubling has been observed during the reduction of oxygen to H_2O_2 at p-GaP and p-GaAs[28,29] (see section IIC). At low intensities, hole injection by $HO_2^{\bullet}$ competes effectively with electron capture. The IMPS response under these conditions has been derived from the following reaction scheme which takes recombination into account.[33,34]

$$h\nu \rightarrow h + e^- \quad (20a)$$

$$O_2 + H^+ + e^- \rightarrow HO_2^{\bullet} \quad (20b)$$

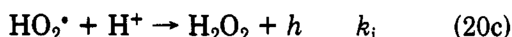

$$HO_2^{\bullet} + H^+ \rightarrow H_2O_2 + h \quad k_i \quad (20c)$$

$$X + e^- \rightarrow Y \quad (20d)$$

$$Y + h \rightarrow X \quad (20e)$$

Figure 28 illustrates the expected potential dependence of the IMPS response (the effect of $R_{sol}C_{sc}$ has been neglected for the sake of clarity). At low values of band bending, recombination dominates and no current doubling can be seen. By contrast, the response in the saturation photocurrent region is free of recombination effects, and the IMPS response is a semicircle in the *lower quadrant*. The low-frequency intercept occurs at 2 as a result of current doubling. At higher frequencies, on the other hand, the relaxation of the intermediate by hole injection is too slow to follow the excitation and the high-frequency intercept is located at unity. The rate constant for majority carrier injection follows directly from the frequency at which the minimum in the semicircle is observed.

Figure 29 shows the experimental results. The rate constant for hole injection was found to be 2.5×10^4 s^{-1},[33,34] suggesting that a thermally activated step is involved. If, as seems probable, the $HO_2^{\bullet}$ intermediate is a surface-bound species located above the valence-band edge, the first-order rate constant k_i for hole injection can be written in the form

$$k_i = \nu \exp(-E_a/kT) \quad (21)$$

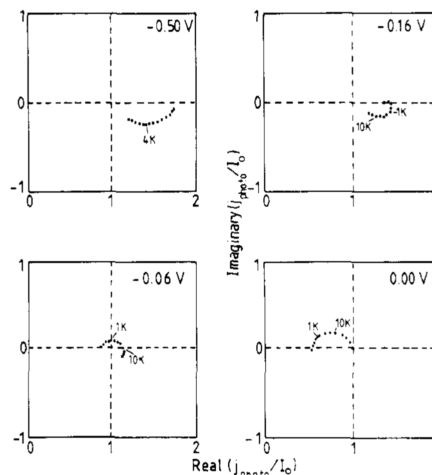

Figure 29. Experimental IMPS plots for p-GaAs in oxygen-saturated 0.5 M $HClO_4$ confirming the progression from recombination control to current doubling predicted by the calculated plots in Figure 28. The rate constant, k_i, for hole injection obtained from the frequency of the minimum is 2.5×10^4 s^{-1}. Potentials vs Pd/H_2.

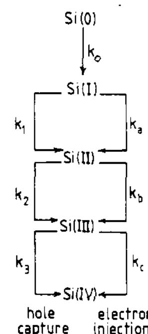

Figure 30. Simplified scheme for the photodissolution of n-Si in NH_4F, contrasting the hole capture and electron injection pathways that couple the different stages of oxidation. The scheme shows that the quantum efficiency can vary between 4 (capture of one hole followed by injection of three electrons) and 1 (capture of four holes) depending on the relative rates of the hole capture and electron injection pathways. Note that hole capture is favored at high intensities.

where ν is a preexponential factor of the order of 10^{12} s^{-1}. It therefore follows from the experimental value of the rate constant that the activation energy E_a is about 0.4 eV.

Photocurrent multiplication during the photodissolution of n-Si in ammonium fluoride solutions (see section IIC) has also been investigated by the IMPS technique.[32] At low light intensities, the quantum efficiency of the photodissolution process approaches 4, whereas at higher intensities it falls to 2. The simplest reaction scheme that can be considered to explain the observed quantum efficiency and its dependence on light intensity is shown in Figure 30 (surface recombination reactions have been omitted for simplicity). It can be seen that quantum efficiencies between 4 and 1 are possible, depending on the relative rates of the hole capture and electron injection routes. The chemical identity of the electron injecting intermediates has not been established, but formally they correspond to the oxidation states of silicon shown in the scheme. The observed dependence of the quantum efficiency follows from the parallel pathways for hole capture and electron injection. The rate of hole capture depends, of course, on the surface hole density. Consequently, hole capture

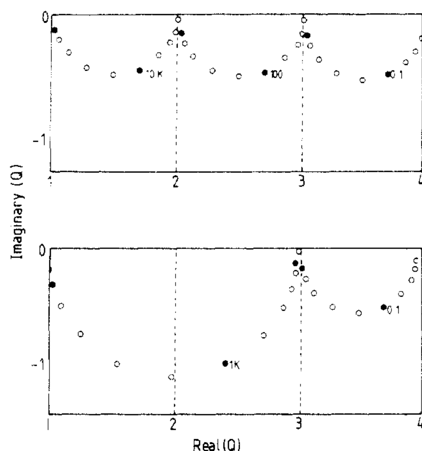

Figure 31. IMPS plots calculated from the reaction scheme in Figure 30 in the low-intensity limit where the hole capture rate constants k_1–k_3 can be neglected: (a) $k_a = 10^6\ s^{-1}$, $k_b = 10^3\ s^{-1}$, $k_c = 1\ s^{-1}$; (b) $k_a = 10^4\ s^{-1}$, $k_b = 10^6\ s^{-1}$, $k_c = 1\ s^{-1}$. It can be seen that the relaxation of intermediate concentrations gives rise to semicircles in the lower quadrant.

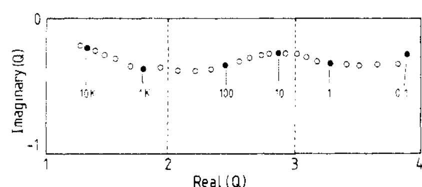

Figure 32. Experimental IMPS response for n-Si in 6.5 M NH_4F (pH 5.4) at 1.5 V vs SCE showing the transition from a quantum efficiency of 4 in the low-frequency limit to 1 at high frequencies as predicted by Figure 30. The results can be fitted with $k_a = 2 \times 10^4\ s^{-1}$, $k_b = 500\ s^{-1}$, $k_c = 0.5\ s^{-1}$, and standard deviation 1.5 kT in the activation energies for electron injection.

will be more favorable at higher light intensities. At low light intensities, on the other hand, hole capture by the intermediates is unable to compete effectively with electron injection, so the quantum efficiency approaches 4.

The theoretical IMPS response has been derived for the low-intensity limit, where hole capture can be neglected. Figure 31 illustrates the way that the electron injection steps give rise to characteristic semicircles in the lower quadrant of the complex plane (an additional semicircle arises from the *RC* time constant of the cell, but it is not shown here). As expected, the low-frequency intercept occurs on the real axis at a quantum efficiency corresponding to the steady-state value of 4. As the frequency is increased, the electron injection steps are progressively "frozen out" until the plot approaches the real axis again at unity. The rate constants for electron injection are given by the frequency at which the semicircles pass through their lowest points.

The IMPS response of n-Si in NH_4F has been measured at low light intensities,[32] and a typical plot is shown in Figure 32 together with a theoretical fit generated by assuming a normal distribution of activation energies for the injection steps. It can be seen that the main features of the predicted response are indeed found experimentally. A more detailed treatment of this system has appeared recently.[111] The results demonstrate the considerable resolving power of the technique. However, more work, for example by in situ infrared spectroscopy, is required in order to identify the intermediates and to follow their relaxation directly.

VIII. Conclusions and Outlook

This survey of non-steady-state aspects of semiconductor photoelectrochemistry has not been exhaustive. Its primary purpose has been to highlight the possibilities and, equally importantly, the limitations of the experimental methods. The kinetic treatments outlined in the review are rather formal; the nature of the surface states responsible for recombination is known only in a few cases, and further work is required to identify intermediates involved in multistep electron-transfer and photodecomposition reactions. Although non-steady-state methods have made important contributions to our understanding, future developments in the analysis of photoelectrochemical processes will also depend on the application of in situ spectroscopic techniques such as Fourier transform[60] and electromodulated infrared,[112,113] which are able to identify surface species. The resolution of the experimental and theoretical problems remains a challenging task.

Acknowledgments. I thank Jianguo Li and Robert Peat for their collaboration in this area of research and the Science and Engineering Council for financial support.

References

(1) Bard, A. J.; Faulkner, L. R. *Electrochemical Methods*; Wiley: New York, 1980.
(2) Southampton Electrochemistry Group. *Instrumental Methods in Electrochemistry*; Ellis Horwood: Chichester, 1985.
(3) Peter, L. M. In *Photocatalysis and the Environment*; NATO ASI Series C, Vol. 237; Schiavello, M., Ed.; Kluwer Academic Publishers: Dordrecht, 1988; p 243.
(4) See e.g.: Delahay, P. *Double Layer and Electrode Kinetics*; Interscience: New York, 1965.
(5) Morrison, S. R. *Electrochemistry of Semiconductors and oxidised Metal Electrodes*; Plenum: New York, 1980.
(6) Myamlin, V. A.; Pleskov, Yu. V. *Electrochemistry of Semiconductors*; Plenum: New York, 1967.
(7) Morrison, S. R. *The Chemical Physics of Surfaces*; Plenum: New York, 1977.
(8) Peter, L. M. In *Electrochemistry*; Specialist Periodical Report; Pletcher, D., Ed.; Royal Society of Chemistry: London, 1984; p 66.
(9) Many, A.; Goldstein, Y.; Grover, N. B. *Semiconductor surfaces*; North Holland: Amsterdam, 1965.
(10) *Semiconductor Photoelectrochemistry*; Pleskov, Yu. V., Gyurevich, Yu. Ya., Eds.; Consultants Bureau: New York, 1986.
(11) Gärtner, W. W. *Phys. Rev.* **1959**, *116*, 84.
(12) Wight, D. R. In *Gallium Arsenide. Materials, Devices and Circuits*; Howes, J. M., Morgan, D. V., Eds.; Wiley: Chichester, 1985; p 1.
(13) Li, J.; Peat, R.; Peter, L. M. *J. Electroanal. Chem. Interfacial Electrochem.* **1984**, *165*, 41.
(14) Peat, R.; Peter, L. M. *Appl. Phys. Lett.* **1987**, *51*, 328.
(15) Peat, R.; Peter, L. M. *Ber. Bunsenges. Phys. Chem.* **1987**, *91*, 381.
(16) Reichman, J. *Appl. Phys. Lett.* **1980**, *36*, 574.
(17) Reichman, J.; Russak, M. A. In *Photoeffects at the semiconductor/electrolyte interface*; Nozik, A. J., Ed.; ACS Symposium Series 146; Electrochemical Society: Princeton, NJ, 1977; p 359.
(18) El Guibaly, F.; Colbow, K.; Funt, B. L. *J. Appl. Phys.* **1981**, *52*, 3480.
(19) Albery, W. J.; Bartlett, P. N.; Hamnett, A.; Dare-Edwards, M. P. *J. Electrochem. Soc.* **1981**, *128*, 1492.
(20) Haneman, D.; McCann, J. F. *Phys. Rev. B* **1982**, *25*, 1241.
(21) Peter, L. M.; Li, J.; Peat, R. *J. Electroanal. Chem. Interfacial Electrochem.* **1984**, *165*, 29.
(22) Morrison, S. R. *Prog. Surf. Sci.* **1971**, *1*, 106.
(23) Freund, T.; Gomes, W. P. *Catal. Rev.* **1969**, *3*, 1.
(24) Dutoit, E. C.; Cardon, F.; Gomes, W. P. *Ber. Bunsenges. Phys. Chem.* **1976**, *80*, 1285.
(25) Gerischer, H.; Rösler, H. *Chem. Ing. Tech. Rev.* **1970**, *4*, 176.
(26) Vanden Berghe, R. A. L.; Gomes, W. P.; Cardon, F. *Z. Phys. Chem. (Munich)* **1974**, *92*, 91.
(27) Memming, R. *J. Electrochem. Soc.* **1969**, *116*, 785.
(28) Li, J.; Peter, L. M. *J. Electroanal. Chem. Interfacial Electrochem.* **1985**, *182*, 399.

(29) Li, J.; Peat, R.; Peter, L. M. *J. Electroanal. Chem. Interfacial Electrochem.* **1986**, *200*, 333.
(30) Matsumura, M.; Morrison, S. R. *J. Electroanal. Chem. Interfacial Electrochem.* **1983**, *144*, 113.
(31) Matsumura, M.; Morrison, S. R. *J. Electroanal. Chem. Interfacial Electrochem.* **1983**, *147*, 157.
(32) Lewerenz, H. J.; Stumper, J.; Peter, L. M. *Phys. Rev. Lett.* **1988**, *61*, 1989.
(33) Peat, R.; Peter, L. M. *Electrochim. Acta* **1986**, *31*, 731.
(34) Peat, R.; Peter, L. M. *J. Electroanal. Chem. Interfacial Electrochem.* **1986**, *209*, 307.
(35) Wilson, R. H. *CRC Crit. Rev. Solid State Mater. Sci.* **1980**, *10*, 2.
(36) Burke, A. A.; Johnson, P. B.; Hobson, W. J.; Ellis, A. B. *J. Appl. Phys.* **1986**, *59*, 1621.
(37) Huppert, D.; Gottesfeld, S.; Harzion, Z.; Evenor, M. In *Ultrafast Phenomena*; Auston, D., Eisenthal, K. B., Eds.; Springer-Verlag: Berlin, 1984; Vol. 4, p 181.
(38) Evenor, M.; Gottesfeld, S.; Harzian, Z.; Huppert, D.; Feldberg, S. W. *J. Phys. Chem.* **1984**, *88*, 6213.
(39) Feldberg, S. W.; Evenor, H.; Huppert, D.; Gottesfeld, S. *J. Electroanal. Chem. Interfacial Electrochem.* **1985**, *185*, 209.
(40) Evenor, M.; Huppert, D.; Gottesfeld, S. *J. Electrochem. Soc.* **1986**, *133*, 296.
(41) Gottesfeld, S. *Ber. Bunsenges. Phys. Chem.* **1987**, *91*, 362.
(42) Benjamin, D.; Huppert, D. *J. Phys. Chem.* **1988**, *92*, 4676.
(43) Vaitkus, J. *Phys. Status Solidi* **1976**, *34A*, 769.
(44) Wilson, R. H. In Reference 17, p 103.
(45) Li, J.; Peter, L. M. *J. Electroanal. Chem. Interfacial Electrochem.* **1985**, *193*, 27.
(46) Marcus, R. A. *J. Phys. Chem.* **1965**, *43*, 679.
(47) Hale, J. M. In *Reactions of molecules at electrodes*; Hush, N. S., Ed.; Wiley Interscience: London, 1971; p 229.
(48) Gmitter, T. T.; Yablonovitch, E.; Heller, A. *J. Electrochem. Soc.* **1988**, *135*, 2392.
(49) Chang, K. C.; Heller, A.; Schwartz, B.; Menezes, S.; Miller, B. *Science* **1977**, *196*, 1097.
(50) Heller, A. In Reference 17, p 57.
(51) Nelson, R. J.; Williams, J. S.; Leamy, H. J.; Miller, B.; Casey, H. C., Jr.; Parkinson, B. A.; Heller, A. *Appl. Phys. Lett.* **1981**, *36*, 76.
(52) Yablonovitch, E.; Allara, D. L.; Chang, C. C.; Gmitter, T.; Bright, T. B. *Phys. Rev. Lett.* **1986**, *57*, 249.
(53) Yablonovitch, E.; Sandroff, C. J.; Bhat, R.; Gmitter, T. *Appl. Phys. Lett.* **1987**, *50*, 1197.
(54) Yablonovitch, E.; Sandroff, C. J.; Bhat, R.; Gmitter, T. *Appl. Phys. Lett.* **1987**, *51*, 439.
(55) Kunst, M.; Tributsch, H. *Chem. Phys. Lett.* **1984**, *105*, 954.
(56) Kunst, M.; Beck, G.; Tributsch, H. *J. Electrochem. Soc.* **1985**, *132*, 700.
(57) Kunst, M.; Jaegermann, W.; Scmeisser, D. *Appl. Phys.* **1987**, *A42*, 5.
(58) Kunst, M.; Beck, G. *J. Appl. Phys.* **1988**, *63*, 1093.
(59) Kunst, M.; Muller, G.; Schmidt, R.; Wetzel, H. *Appl. Phys.* **1988**, *A46*, 77.
(60) Peter, L. M.; Blackwood, D. J.; Pons, S. B. *Phys. Rev. Lett.* **1989**, *62*, 308.
(61) Tiedje, T.; Colbow, K. M.; Rogers, D.; Fu, Z.; Eberhardt, W. *J. Vac. Sci. Technol.* **1989**, *B7*, 837.
(62) Carpenter, M. S.; Melloch, M. R.; Cowans, B. A.; Dordas, Z.; Delgass, W. N. *J. Vac. Sci. Technol.* **1989**, *B7*, 845.
(63) Richardson, J. H.; Deutscher, S. B.; Maddix, A. S.; Harrer, J. E.; Schelzinger, D. C.; Perone, S. P. *J. Electroanal. Chem. Interfacial Electrochem.* **1980**, *109*, 95.
(64) Deutscher, S. B.; Richardson, J. H.; Perone, S. P.; Rosenthal, J.; Ziemer, J. *Faraday Discuss. Chem. Soc.* **1980**, *70*, 1.
(65) Perone, S. P.; Richardson, J. H.; Deutscher, S. B.; Rosenthal, J.; Zeimer, J. N. *Faraday Discuss. Chem. Soc.* **1980**, *70*, 35.
(66) Perone, S. P.; Richardson, J. H.; Deutscher, S. B.; Rosenthal, J.; Zeimer, J. N. *J. Electrochem. Soc.* **1980**, *127*, 2580.
(67) Huppert, D.; Kolodny, E. *J. Chem. Phys.* **1981**, *63*, 401.
(68) Perone, S. P.; Richardson, J. H.; Deutscher, S. B. *J. Phys. Chem.* **1981**, *85*, 341.
(69) Kawai, T.; Tributsch, H.; Sakata, T. *Chem. Phys. Lett.* **1980**, *69*, 336.
(70) Richardson, J. H.; Perone, S. P.; Deutscher, S. B. *J. Phys. Chem.* **1981**, *85*, 341.
(71) Harzion, Z.; Croituru, N.; Gottesfeld, S. *J. Electrochem. Soc.* **1981**, *128*, 551.
(72) Kamat, P. V.; Fox, M. A. *J. Phys. Chem.* **1983**, *87*, 59.
(73) Harzion, Z.; Croituru, N.; Huppert, D.; Gottesfeld, S. *J. Electroanal. Chem. Interfacial Electrochem.* **1983**, *150*, 571.
(74) Gottesfeld, S.; Feldberg, S. W. *J. Electroanal. Chem. Interfacial Electrochem.* **1983**, *146*, 47.
(75) Prybyla, S.; Struve, W. S.; Parkinson, B. A. *J. Electrochem. Soc.* **1984**, *131*, 1587.
(76) Jaegermann, W. *J. Phys. Chem.* **1984**, *88*, 5309.
(77) Jaegermann, W.; Sakata, T.; Janata, E.; Tributsch, H. *J. Electroanal. Chem. Interfacial Electrochem.* **1985**, *189*, 65.
(78) Wilson, R. H.; Sakata, T.; Kawai, T.; Hashimoto, K. J. *J. Electrochem. Soc.* **1985**, *132*, 1082.
(79) Hartig, K. J.; Grabner, G.; Getoff, N.; Popikirov, G.; Kanet, S. *Ber. Bunsenges. Phys. Chem.* **1985**, *89*, 831.
(80) Itoh, K.; Nakao, M.; Honda, K. *J. Appl. Phys.* **1983**, *57*, 5493.
(81) Cook, R. L.; Dempsey, P. F.; Sammells, A. F. *J. Electrochem. Soc.* **1986**, *133*, 1821.
(82) Cook, R. L.; Dempsey, P. F.; Sammels, A. F. *J. Electrochem. Soc.* **1986**, *133*, 2287.
(83) Bitterling, K.; Willig, F. *J. Electroanal. Chem. Interfacial Electrochem.* **1986**, *204*, 211.
(84) Sakata, T.; Janata, E.; Jaegermann, W.; Tributsch, H. *J. Electrochem. Soc.* **1986**, *133*, 339.
(85) Bitterling, K.; Willig, F.; Decker, F. *J. Electrochem. Soc.* **1987**, *228*, 29.
(86) Willig, F. *Ber. Bunsenges. Phys. Chem.* **1988**, *92*, 1312.
(87) Norton, A. P.; Bernasek, S. L.; Bocarsly, A. B. *J. Phys. Chem.* **1988**, *92*, 6009.
(88) Peter, L. M.; Lewerenz, H. J.; Stumper, J. *Electrochim. Acta*, in press.
(89) Frippiat, A.; Kirsch de Mesmaeker, A.; Nasieslki, J. *J. Electrochem. Soc.* **1983**, *130*, 239.
(90) Frippiat, A.; Kirsch de Mesmaeker, A. *J. Phys. Chem.* **1985**, *89*, 1285.
(91) Fichou, D.; Kirsch de Mesmaeker, A. *Chem. Phys. Lett.* **1986**, *132*, 128.
(92) Fichou, A.; Kirsch de Mesmaeker, A. *J. Electroanal. Chem. Interfacial Electrochem.* **1986**, *215*, 161.
(93) Kirsch de Mesmaeker, A.; Rochus-Dewitt, M.; Nasieslki, J. *J. Phys. Chem.* **1986**, *90*, 6657.
(94) Abrantes, L. M.; Peter, L. M. *J. Electroanal. Chem. Interfacial Electrochem.* **1983**, *150*, 593.
(95) Peter, L. M.; Li, J.; Peat, R. *J. Electroanal. Chem. Interfacial Electrochem.* **1984**, *165*, 29.
(96) Ginley, D. S.; Butler, M. A. *J. Electrochem. Soc.* **1978**, *125*, 1968.
(97) Albery, W. J.; Bartlett, P. N. *J. Electrochem. Soc.* **1982**, *129*, 2254.
(98) Iwanski, P.; Curran, J. S.; Gissler, W.; Memming, R. *J. Electrochem. Soc.* **1981**, *128*, 2128.
(99) Sagara, T.; Sukigara, M. *J. Electrochem. Soc.* **1988**, *135*, 363.
(100) Nogami, G.; Nishiyama, Y. *J. Electrochem. Soc.* **1988**, *135*, 3038.
(101) Pujadas, M.; Salvador, P. *J. Electrochem. Soc.* **1989**, *136*, 716.
(102) Peter, L. M. In *Trends in Interfacial Electrochemistry*; NATO ASI Series; Silva, F. A., Ed.; Reidel: Dordrecht, 1986; p 523.
(103) Li, J.; Peter, L. M. *J. Electroanal. Chem. Interfacial Electrochem.* **1985**, *193*, 27.
(104) Li, J.; Peat, R.; Peter, L. M. *J. Electroanal. Chem. Interfacial Electrochem.* **1986**, *199*, 1.
(105) Kaminiecki, E. *J. Vac. Sci. Technol.* **1982**, *20*, 811.
(106) Kaminiecki, E. *J. Appl. Phys.* **1983**, *54*, 6481.
(107) Albery, W. J.; Bartlett, P. N.; Wilde, C. P. *J. Electrochem. Soc.* **1987**, *134*, 2486.
(108) Cardon, F.; Gomes, W. P. *Surf. Sci.* **1971**, *27*, 286.
(109) Gomes, W. P.; Cardon, F. *J. Solid State Chem.* **1971**, *3*, 125.
(110) Peat, R.; Peter, L. M. *J. Electroanal. Chem. Interfacial Electrochem.* **1987**, *228*, 351.
(111) Borazio, A. M.; Peter, L. M.; Stumper, J.; Lewerenz, H. J. *J. Electroanal. Chem. Interfacial Electrochem.*, in press.
(112) Venkateswara Rao, A.; Chalzaviel, J. N. *J. Electrochem. Soc.* **1987**, *34*, 2777.
(113) Ventkateswara Rao, A.; Chalzalviel, J. N.; Ozanam, F. *J. Appl. Phys.* **1986**, *60*, 696.